Petroleum Geoscience

Reservoir stress path characterization and its implications for fluid-flow production simulations

J. M. Segura, Q. J. Fisher, A. J. L. Crook, et al.

Email alerting service	click here to receive free e-mail alerts when new articles cite this article
Permission request	click here to seek permission to re-use all or part of this article
Subscribe	click here to subscribe to Petroleum Geoscience or the Lyell Collection

Notes

Lyell Collection

Reservoir stress path characterization and its implications for fluid-flow production simulations

J. M. Segura[1], Q. J. Fisher[1,*], A. J. L. Crook[2], M. Dutko[2], J. G. Yu[2], S. Skachkov[1], D. A. Angus[1,3], J. P. Verdon[3] and J-M. Kendall[3]

[1]*Centre for Integrated Petroleum Engineering and Geosciences, University of Leeds, Leeds LS2 9JT, UK*
[2]*Rockfield Software Ltd, Ethos Building, Kings Road, Swansea SA1 8AS, UK*
[3]*Department of Earth Sciences, University of Bristol, Wills Memorial Building, Queen's Road, Bristol BS8 1RJ, UK*
[*]*Corresponding author (e-mail: Q.J.Fisher@leeds.ac.uk)*

ABSTRACT: The reduction of fluid pressure during reservoir production promotes changes in the effective and total stress distribution within the reservoir and the surrounding strata. This stress evolution is responsible for many problems encountered during production (e.g. fault reactivation, casing deformation). This work presents the results of an extensive series of 3D numerical hydro-mechanical coupled analyses that study the influence of reservoir geometry and material properties on the reservoir stress path. The stress path is defined in terms of parameters that quantify the amount of stress arching and stress anisotropy that occur during reservoir production. The coupled simulations are performed by explicitly coupling independent commercial geomechanical and flow simulators. It is shown that stress arching is important in reservoirs with low aspect ratios that are less stiff than the bounding material. In such cases, the stresses will not significantly evolve in the reservoir, and stress evolution occurs in the over- and sideburden. Stiff reservoirs, relative to the bounding rock, exhibit negligible stress arching regardless of the geometry. Stress anisotropy reduces with reduction of the Young's modulus of the bounding material, especially for low aspect ratio reservoirs, but as the reservoir extends in either or both of the horizontal directions, the reservoir deforms uniaxially and the horizontal stress evolution is governed by the Poisson's ratio of the reservoir. Furthermore, the effect of the stress path parameters is introduced in the calculation of pore volume multiplier tables to improve non-coupled simulations, which otherwise overestimate the average reservoir pore pressure drawdown when stress arching is taking place.

KEYWORDS: *hydro-mechanical coupling, stress path, stress arching, pore volume multiplier*

INTRODUCTION

Change in reservoir pore pressure due to hydrocarbon production promotes changes not only in the effective stress, but also in the total stress distribution acting on the reservoir and the surrounding rock. If the total stress remains constant, the change in effective stress in the reservoir is isotropic, and the stress path is horizontal in the p'–q plane. In other words, in a simplified 2D representation of the stress state, the Mohr circle would simply translate with no change in size (Fig. 1a). In the general case, fluid pressure reduction is accompanied by a reduction in the total horizontal stress, termed 'field scale σ_h/p coupling' (Hillis 2001), which leads to the development of deviatoric stresses and the associated expansion of the Mohr Coulomb circle (Fig. 1b).

The total vertical stress is commonly assumed to be defined by the weight of the overburden and to remain unchanged during reservoir production. However, this ideal case is not valid when stress arching occurs, i.e. when part of the overburden weight is transmitted to the sideburden during reservoir compaction (Khan *et al.* 2000; Sayers & Schutjens 2007).

Estimating the stress evolution during reservoir production is important for predicting phenomena such as the generation or reactivation of faults, pore collapse, bedding-parallel slip, casing deformation, or seismic activity (Van Eijs *et al.* 2006; Sayers & Schutjens 2007; Angus *et al.* 2010; Verdon *et al.* 2010). The stress state is also a key input in designing hydraulic fracture stimulation plans, as the stress state determines the injection fluid pressure necessary to fracture the rock as well as the fracture propagation direction. Furthermore, in geophysical studies, identification of relative change in the horizontal and vertical stresses is extremely beneficial, as a larger change in total horizontal stress than the accompanying change in
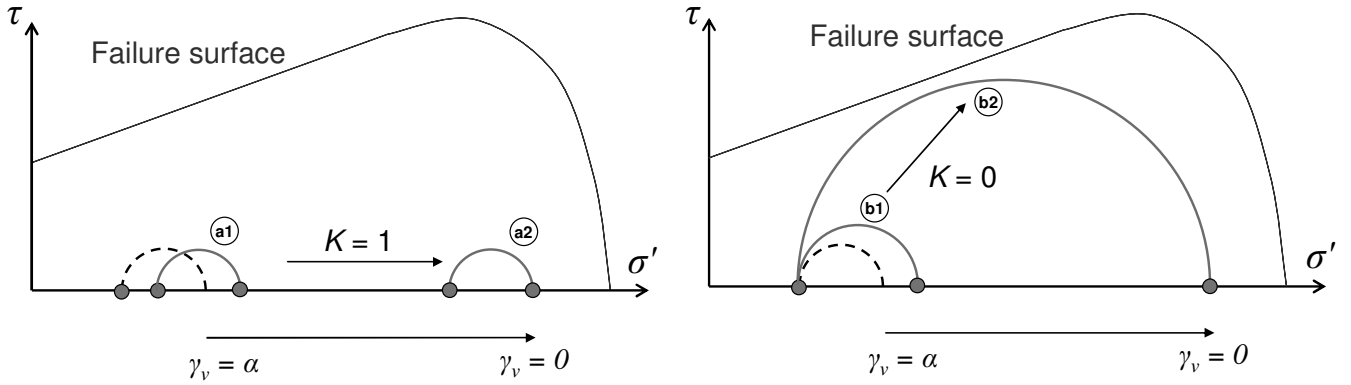
Fig. 1. Mohr circle evolution during reservoir depletion as a function of K and γ_v if (a) $K=1$ or (b) $K=0$.

vertical stress may lead to significant changes in elastic-wave anisotropy (Sayers 2006; Verdon *et al.* 2008).

Numerical and theoretical studies exist in the literature that analyse the controls of the reservoir geometry and the material properties on the reservoir stress path during production. A stiff overburden (compared to the reservoir stiffness) will promote stress arching as the reservoir compacts (Sayers & Schutjens 2007) and stress changes will occur more in the overburden than within the reservoir (Alassi *et al.* 2006). Khan *et al.* (2000) and Sayers (2006) show that K, the stress path parameter defined in equation (5), tends towards the oedometric value as the aspect ratio of reservoir length to thickness increases for isotropic reservoir properties. These studies are based on 2D or axisymmetrical reservoir geometries (e.g. cylindrical or ellipsoidal).

This article analyses the effect of 3D reservoir geometry on the reservoir stress path during production. A series of numerical studies are performed to predict the stress path parameters as a function of 3D reservoir geometry and for contrasts in elastic material properties in the reservoir and the bounding material. These results are valuable for prediction of the stress evolution during production, but, also, may be used to improve the accuracy of fluid flow simulations. This is achieved by introducing the influence of the stress path parameters in the pore volume multipliers tables used by standard production simulation modelling software packages, and thereby providing a more realistic spatial distribution of porosity change during production.

This paper begins by defining the stress path parameters; it then considers the effect of reservoir geometry and material properties on the stress path and the final section discusses the effect of the stress path parameters on fluid flow simulations.

DEFINITION OF STRESS PATH PARAMETERS

The stress evolution during reservoir production depends mainly on the initial stress state prior to production, the material properties (both reservoir and bounding material) and the reservoir geometry, and can be defined in terms of the 'reservoir stress path parameters'. In this definition it is assumed that the maximum and minimum principal stresses are vertical and horizontal respectively, i.e. uniaxial burial/extensional stress regime where $\sigma'_v > \sigma'_H \geq \sigma'_h$ and σ'_v, σ'_H and σ'_h, are the effective vertical, maximum and minimum horizontal stresses respectively.

A pressure drop Δp is considered due to fluid withdrawal from a reservoir, which according to Terzaghi's generalized effective stress principle (Terzaghi 1943; Biot & Willis 1957) promotes a change of the effective and total stresses:

$$\Delta\sigma'_v = \Delta\sigma_v - a\Delta p, \tag{1}$$

$$\Delta\sigma'_h = \Delta\sigma_h - a\Delta p, \tag{2}$$

where $\Delta\sigma'_v$ and $\Delta\sigma'_h$ are the incremental effective vertical and minimum horizontal stresses respectively, $\Delta\sigma_v$ and $\Delta\sigma_h$ are the incremental total stress values, and a is the Biot's parameter (Biot & Willis 1957). Usually, a is assumed to be equal to 1. However, in reality it may vary between 0 and 1 with typical values being between 0.3 and 1 (e.g. Fatt 1959; Franquet & Abass 1999).

Three 'stress path parameters' are defined, which describe the evolution of the stress state in the reservoir during production:

$$\gamma_v = \frac{\Delta\sigma_v}{\Delta p}, \tag{3}$$

$$\gamma_h = \frac{\Delta\sigma_h}{\Delta p}, \tag{4}$$

and

$$K = \frac{\Delta\sigma'_h}{\Delta\sigma'_v} = \frac{\gamma_h - a}{\gamma_v - a}. \tag{5}$$

Here we refer to γ_v as the 'stress arching parameter', γ_h as the 'horizontal stress path parameter' and K as the 'deviatoric stress path parameter'. Parameter γ_h is usually estimated in the field with hydraulic fracturing tests (e.g. micro-frac or extended leak-off tests). Equation (5) shows that only two out of the three stress path parameters are independent. Parameters γ_v and K are chosen in this work as the reference parameters to study the stress path.

The parameter γ_v describes the amount of stress arching during production. If γ_v is high, stress arching occurs and the effective stress evolution is minimal in the reservoir and is mostly manifested in the overburden in the form of unloading (vertical stress decreases), and in the sideburden in the form of loading.

The parameter K describes the development of stress anisotropy, and therefore the likelihood of shear failure or pore collapse in the material. Lower values of K correspond to lower changes in horizontal effective stress than in vertical effective stress, or in other words, to an increase in stress anisotropy. Stress anisotropy can only increase if the vertical effective stress increases, or more specifically providing stress arching does not occur (i.e. with low values γ_v).

In terms of a Mohr circle representation of the stress state, K defines the new size of the circle and γ_v defines the new right

Table 1. *Data on the horizontal stress path parameter γ_h as derived from the literature*

Reservoir	Lithology	γ_h	Reference
Waskom field	Sandstone (Travis Peak)	0.46	Holditch *et al.* (1987)
Several: West Texas	Sandstone (Vicksburg)	0.38–0.63	Salz (1977)
Unknown	Unfaulted poorly lithified sand (probably Mid-Jurassic)	0.7	Santarelli *et al.* (1998)
Unknown	Faulted poorly lithified sand	0.42	Santarelli *et al.* (1998)
Ekofisk	Chalk	0.8	Teufel *et al.* (1991)
Groningen	Lithified sandstone (Rotliegend)	0.2–0.6	Hettema *et al.* (1998)
Magnus	Lithified sandstone (Jurassic)	0.68	Shepherd (1991)
West Sole	Lithified sandstone (Rotliegend)	1.18	Winter & King (1991)
Wytch farm	Triassic sandstone	0.65	Addis (1997)
Venture Field, Nova Scotia	Sandstone	0.56	Ervine & Bell (1987)

hand side coordinate of the circle. This is summarized in Figure 1.

a. If $K \rightarrow 1$, the development of deviatoric stress is minimum and the Mohr circle tends to translate, giving:

- circle a1 with little translation if stress arching occurs, i.e. $\gamma_v \rightarrow a$;
- circle a2 with large translation if stress arching does not occur, i.e. $\gamma_v \rightarrow 0$. This case is more prone to pore collapse.

b. If $K \rightarrow 0$, the development of deviatoric stress will be maximum, giving:

- circle b1 with little growth if stress arching occurs, i.e. $\gamma_v \rightarrow a$;
- circle b2 with maximum growth if stress arching does not occur, i.e. $\gamma_v \rightarrow 0$. This case is more prone to shear failure, although that depends on the initial stress state and the material properties.

There is commonly a great deal of inconsistency between the use and definition of the stress path parameters in the reservoir engineering literature, so great care needs to be taken when collating data. Whereas some authors use K to denote the 'stress path' (Khan *et al.* 2000; Sayers 2006), others use γ_h (Santarelli *et al.* 1998; Goulty 2003). Stress path results can refer to experimental studies or to field data obtained using hydrofracturing type tests. In many situations it is assumed that $\gamma_v = 0$ (i.e. no stress arching effect) and in this case K and γ_h are equivalent (equation 5).

As summarized by Goulty (2003), K is in the range of 0.4–0.6 during the normal compaction of chalk. K commonly has values around 0.3–0.4 for sands, 0.7 or greater for clays, and values between these extremes in silts (Jones 1994). Hettema *et al.* (1998) analysed a discrepancy between the stress path calculated theoretically assuming uniaxial strain conditions ($\gamma_h = 0.8$) and the stress path inferred from the Groningen field data ($\gamma_h = 0.4$). A summary of measured stress path data from some producing petroleum reservoirs is presented in Table 1.

In terms of controls on reservoir stress path, a commonly used simplification is that the rock response is poroelastic and deforms uniaxially during production (i.e. passive basin or oedometric). In this case, the parameter K is a function of the rock Poisson's ratio v:

$$K = \frac{v}{1-v}, \tag{6}$$

and if no stress arching is taking place ($\gamma_v = 0$):

$$\gamma_h = a\frac{1-2v}{1-v}. \tag{7}$$

In faulted reservoirs, the stress path can be controlled by critically-stressed faults and their (residual) friction angle (Addis *et al.* 1996, 1998; Wu *et al.* 1998).

For some overconsolidated fine-grained sediments, it has been demonstrated experimentally under oedometric conditions that the stress path parameter K evolves from the elastic value in equation (6) to an asymptotic value corresponding to the uniaxial plastic consolidation of the material (Pouya *et al.* 1998).

EFFECT OF RESERVOIR GEOMETRY AND MATERIAL PROPERTIES ON RESERVOIR STRESS PATH

A series of 3D numerical coupled hydro-mechanical analyses has been performed to study the effect of reservoir geometry and material properties on the development of stress arching and stress anisotropy during production. The values for the stress path parameters γ_v and K (equations 3 and 5) have been calculated numerically, and given as a function of reservoir aspect ratios and material properties.

The numerical analyses consider a pressure drop of 10 MPa within a reservoir located at 3048 m (10 000 ft) depth. Ten reservoir geometries are analysed (Fig. 2), which combine low, mid and high aspect ratios in the two vertical planes XZ and YZ, covering extreme cases such as small, large and thin reservoirs, and all the intermediate shapes. A small reservoir (aspect ratio 5 in XZ and YZ) or a thin plank-type reservoir (aspect ratio 100 in XZ and 5 YZ) are analogues of highly compartmentalized reservoirs, and a large reservoir (aspect ratio 100 in XZ and YZ) can be associated with non-compartmentalized blanket-type reservoirs. The influence of the bounding and reservoir Young's modulus and Poisson's ratio on the stress path is studied for each geometry. The well is located in the centre of the reservoirs. The remaining material parameters and boundary conditions are fixed and correspond to a case study proposed by Dean *et al.* (2003).

The simulations are performed using a code that explicitly couples the TEMPEST production simulation model (Roxar Ltd) for the flow calculations with ELFEN finite element program (Rockfield Software Ltd) for the geomechanical simulations. An MPI interface developed by Rockfield Software Ltd controls the transfer of fluid pressure data from TEMPEST to ELFEN, pore volume multiplier data from ELFEN to TEMPEST, and also at which time-steps it is
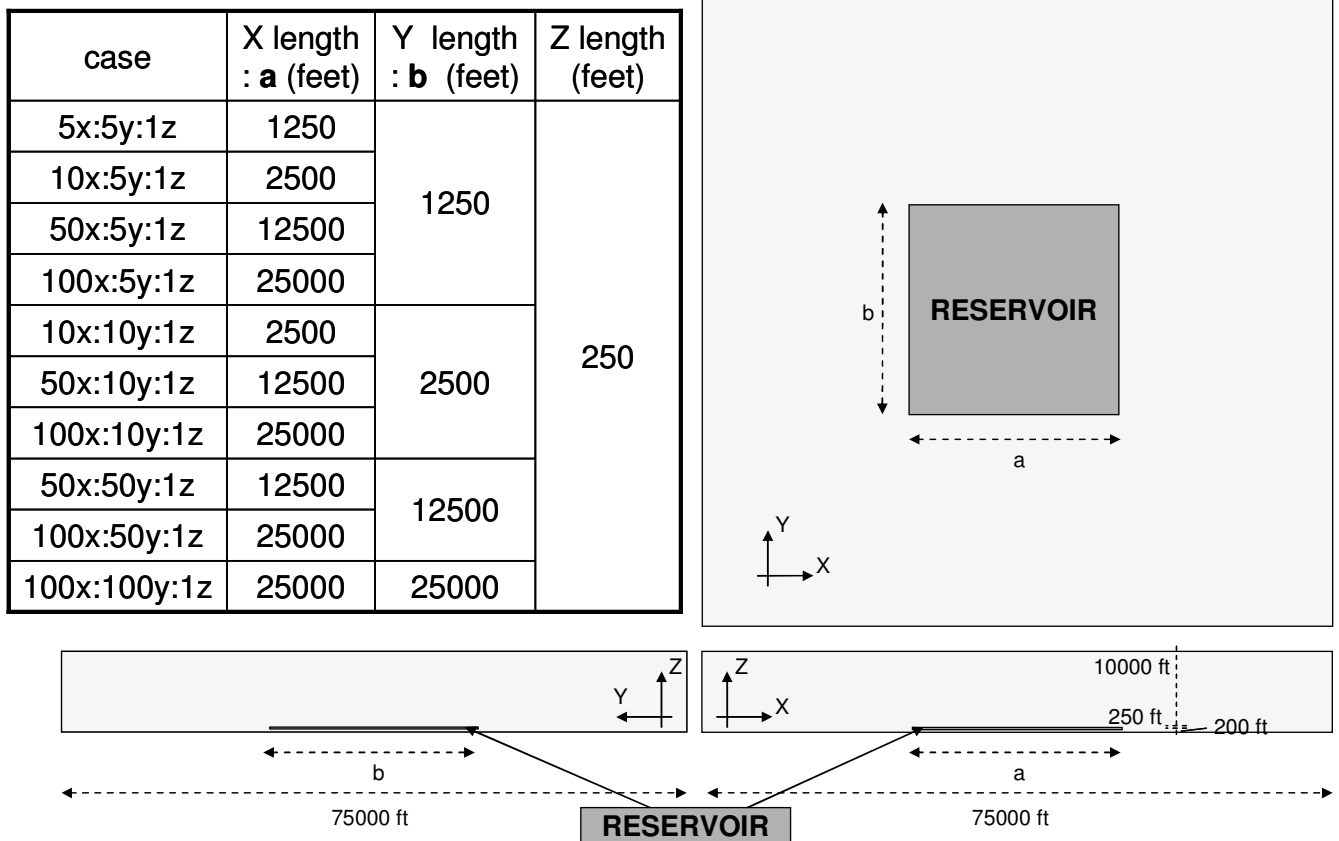
Fig. 2. Reservoir geometries/dimensions analysed.

necessary to make this information exchange (Crook & Dutko pers. comm. 2006).

The results shown in this section extend the 2D and axisymmetric studies that exist in the literature (Khan & Teufel 1996; Khan *et al.* 2000; Alassi *et al.* 2006; Sayers 2006; Sayers & Schutjens 2007) into three dimensions, showing, when comparable, a good agreement with their results as explained next.

Influence of Young's modulus on γ_v and K

Two groups of simulations are performed to study the effect of the reservoir and the bounding rock Young's moduli. The first group fixes the reservoir Young's modulus ($E_r = 6.89$ GPa) and analyses the effect of varying the bounding material Young's modulus (E_b). The second group fixes $E_b = 6.89$ GPa

and varies E_r. For a given geometry and for a given ratio E_r/E_b, the results, in terms of stress path parameters, are very similar regardless of the absolute value of the moduli (average difference lower than 1%). The numerical results, therefore, are presented in terms of the ratio E_r/E_b.

Figure 3 provides the values of γ_v and K in the well zone as a function of the ratio E_r/E_b and the reservoir geometry. The axes in Figure 3 represent:

- x: aspect ratio in the X direction (i.e. reservoir length in X over thickness in Z; e.g. 50 for a reservoir that is 50 times longer in X than thick in Z);
- y: aspect ratio in the Y direction;
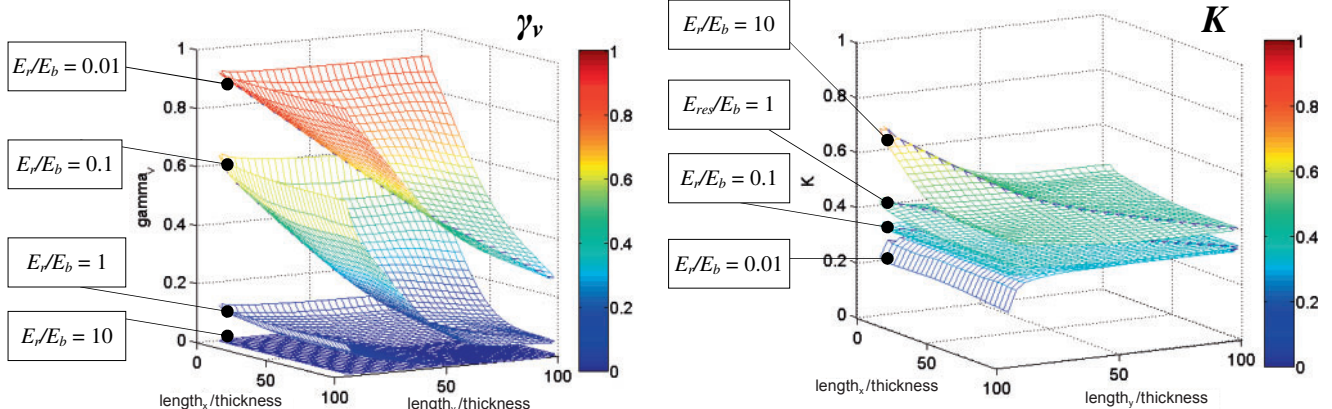- z: stress path parameter value for the geometry with aspect ratios (x,y).

Fig. 3. Parameters (a) γ_v and (b) K as a function of reservoir geometry and E_r/E_b.
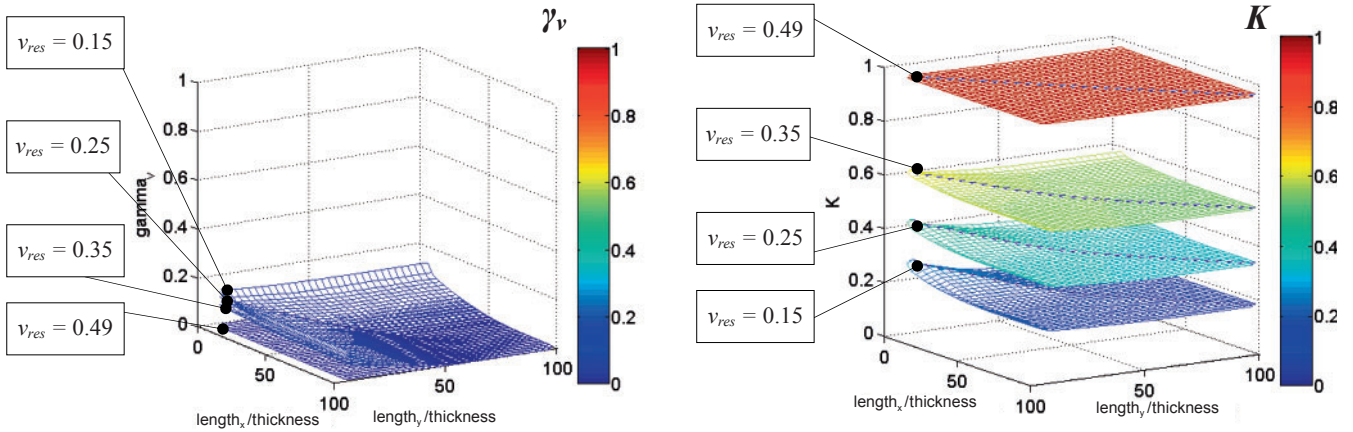
Fig. 4. Parameters (a) γ_v and (b) K as a function of reservoir geometry and v_r.

Figure 3a shows that γ_v is very low if the reservoir Young's modulus is 10 times larger than that of the bounding material ($E_r/E_b=10$), and there is negligible stress arching for all geometries. As the reservoir stiffness is decreased, γ_v increases, especially for reservoirs with low aspect ratios in either one or both directions. γ_v values are close to one when the reservoir is much softer ($E_r/E_b = 0.01$) and is either small or plank-like (i.e. small aspect ratios in X or/and in Y); in such reservoirs, stress arching is significant and the weight of the overburden is partly supported by the sideburden.

Figure 3b shows that for a contrast $E_r/E_b=10$, K is high for small reservoirs and tends to decrease towards the oedometric value as either or both of the horizontal dimensions of the reservoir increases. The effect of reservoir geometry on K is not as pronounced as for γ_v, and the oedometric hypothesis seems a good approximation unless the reservoir aspect ratio in the two directions is small and the contrast in elastic properties is large. Similar plots to Figure 3 have been produced for other areas of the reservoir (not shown), and average values for a reservoir may be calculated. The stress parameter evolution in the well area, however, is usually the most critical and is the most useful when predicting well failure and for hydraulic fracturing design.

Influence of Poisson's ratio on γ_v and K

Figure 4 provides the stress path parameters γ_v (Fig. 4a) and K (Fig. 4b) in the well zone as a function of the reservoir geometry and reservoir Poisson's ratio, for which four values have been considered ($v_r = 0.15$; 0.25; 0.35; 0.49). In this group

of simulations a Young's modulus of 6.89 GPa has been used for the reservoir and bounding material; the bounding material Poisson's ratio is $v_b = 0.25$.

Figure 4a shows that the value of v_r does not significantly alter the parameter γ_v for the studied ratio $E_r/E_b=1$. Increasing v_r reduces stress arching because the reservoir is less compressible. On the other hand, K is significantly influenced by v_r and it tends to the uniaxial compaction value (equation 6) independently of the geometry as v_r increases. Reservoirs with low aspect ratios exhibit higher K than the uniaxial compaction value if v_r is small.

Simulations have also been performed with a fixed value of the reservoir Poisson's ratio ($v_r = 0.25$), and for three values of the bounding material Poisson's ratio ($v_b = 0.125$; 0.25; 0.49). The influence of v_b in the stress path parameters is very small for the studied ratio $E_r/E_b=1$, obtaining almost identical surfaces regardless of v_b as shown in Figures 5 (a and b).

Vertical sections of the surfaces in Figures 3, 4 and 5 along the line $x = y$ give curves that compare well with the 2D and axisymmetric results existing in the literature (Khan & Teufel 1996; Khan *et al.* 2000; Alassi *et al.* 2006; Sayers 2006; Sayers & Schutjens 2007).

Figures 3, 4 and 5 provide an estimate of the stress path parameters K and γ_v in the neighbourhood of the well as a function of the reservoir aspect ratio and the elastic constant contrast between the reservoir and the bounding material. They therefore provide estimates and guidelines on the expected likelihood of failure type (shear or compaction) and stress arching. They can be used for any generic reservoir provided that its behaviour is approximated to an analogous
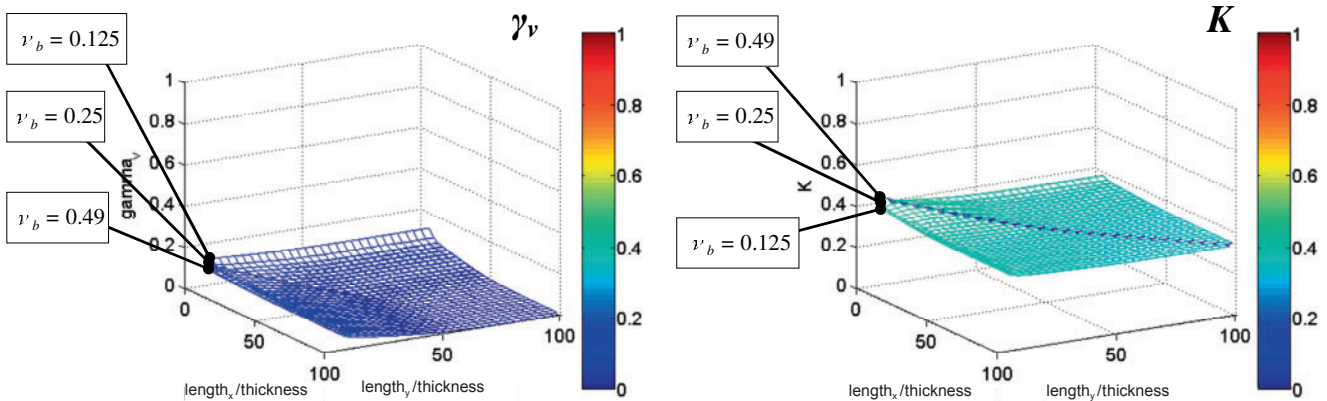

Fig. 5. Parameters (a) γ_v and (b) K as a function of reservoir geometry and v_b.

linear elastic behaviour and its geometry is close to a hexahedral shape.

IMPROVING FLUID FLOW SIMULATIONS BASED ON THE STRESS PATH PARAMETERS

Introduction

Coupled geomechanical/fluid flow simulation is becoming more regularly adopted to predict the evolution of material, pore pressure and stress state in reservoir related applications, e.g. subsidence, compaction drive, fault reactivation, hydraulic stimulation, etc. resulting in a variety of workflows and toolkits such as coupled geomechanical/fluid flow simulations (e.g. Fredrich *et al.* 2000; Kristiansen 2009; Palmer *et al.* 2002; Settari *et al.* 2009). A number of different coupling schemes have been proposed, ranging from coupling of standalone reservoir and geomechanical models (either explicitly or implicitly), to fully coupled models where the fluid flow and geomechanical fields are solved simultaneously.

Coupled simulation of reservoir production is much more resource intensive, both in terms of model building and characterization and also computational requirements (as the surrounding sideburden and overburden must be represented in the model). Consequently, much attention has been focused on:

- Identifying the conditions where coupled geomechanical/ fluid flow analysis is required and the accuracy of the coupling method (e.g. Dean *et al.* 2003; Gai *et al.* 2005; Gutierrez & Lewis 1998; Osorio *et al.* 1999; Settari & Walters 1999; Tran *et al.* 2005; Segura & Carol 2008).
- Developing workflows which facilitate improved accuracy of non-coupled fluid flow simulations via conditioning the pore volume multiplier tables which are used to represent the influence of reservoir compaction (e.g. Pettersen & Kristiansen 2009).

The computational savings furnished by the latter strategies have a huge potential benefit when history-matching reservoir production, as simulation may be performed either (a) using non-coupled flow simulations alone, or (b) using one or two coupled geomechanical/flow simulations to condition the pore volume multiplier tables for non-coupled reservoir flow simulations (e.g. Pettersen 2008; Pettersen & Kristiansen 2009). This section presents a simple procedure to improve non-coupled simulations by introducing the effect of the stress path parameters in the look-up tables of pore volume multipliers.

Methodology

In non-coupled fluid flow simulation of reservoir production, the effect of the reservoir compaction is generally introduced via look-up tables of pore volume multipliers (PVM), that relate the change in pore volume within the reservoir to the change in reservoir pore pressure. These tables are commonly based on observations in oedometric experimental tests. This section studies the accuracy of non-coupled simulations based on these assumptions compared to coupled fluid flow–geomechanical models, and demonstrates the improvement in accuracy of non-coupled reservoir simulations, when the effect of the stress path parameters are introduced in the pore volume multiplier table.

Reservoir production is solved using a coupled fluid flow-geomechanics code and a standalone fluid flow simulator. The comparison between both solutions is made in terms of the

hydrocarbon average pore pressure. The coupled simulation is performed using the same explicit coupling scheme between TEMPEST and ELFEN used in Section 2 (Crook & Dutko pers. comm. 2006). The non-coupled simulation is performed using the TEMPEST reservoir production simulator. The analysis considers an idealized chalk reservoir with mudstone overburden and sideburden. Consequently, due to the high porosity/low strength of the chalk, an elasto-plastic model with non-linear elasticity is used to represent the chalk, as opposed to the idealized linear elastic model adopted in the previous section. The look-up table of PVM against pore pressure for the fluid flow simulation is obtained by conducting a numerical consolidation test. This consolidation test is performed in two configurations:

- assuming uniaxial compaction due to pore pressure drawdown with constant overburden stress; and
- assuming uniaxial compaction due to pore pressure drawdown with reducing overburden stress based on the average stress path for the reservoir.

This approach for evaluating the impact of stress arching on PVM table differs from the approach proposed by Schutjens *et al.* (2004), where the ratio K is used to correct the PVM table, which requires explicit definition of both $\Delta\sigma'_v$ and $\Delta\sigma'_h$ as a function of Δp. In this case only $\Delta\sigma'_v$ is prescribed and $\Delta\sigma'_h$ is evaluated by ensuring consistency of the stress and material state during reservoir depletion.

Geometry and materials

A large blanket-type reservoir (dimensions $100x:100y:1z$ in Fig. 2) is used for the sake of generalization. The material models correspond to a mudstone and a chalk from the North Sea. A weak chalk that undergoes large amounts of pore collapse during production is considered for the reservoir, so moderate stress arching is expected to occur in this case. The bounding material is considered to be a mudstone.

The constitutive model used for both rocks is a critical state-based model specially developed for soft rocks (Crook *et al.* 2002), which can simulate both shear failure localization and pore collapse due to compaction. A Cam-Clay type expression is considered for the definition of the elasticity:

$$K = K_0 + \frac{1}{\kappa}\left(\frac{1}{1-\phi}\right)\sigma'_m, \qquad (8)$$

where K is the bulk modulus, κ a model parameter, ϕ the porosity and σ'_m the effective mean stress.

The reservoir initial Young's modulus (before starting production) is approximately $E = 6.8$ GPa. The Poisson's ratio is $v = 0.2$.

The bounding material exhibits zero plastic deformation during the simulations; i.e. it behaves elastically, with a depth variable Young's modulus derived from equation (8) with $K_0 = 1000$ MPa and $\kappa = 0.01$ and that ranges from approximately 2GPa at the top to 6.8GPa at the bottom of the model. The Poisson's ratio is $v = 0.2$.

Generation of the PVM tables

A numerical compaction simulation is performed to obtain the PVM table that will be introduced into the flow simulator input data for the non-coupled simulation. Figure 6 shows a schematic of the boundary, initial and loading conditions. The specimen is loaded by an upper distributed load and is assigned an initial pore pressure, both corresponding to the average
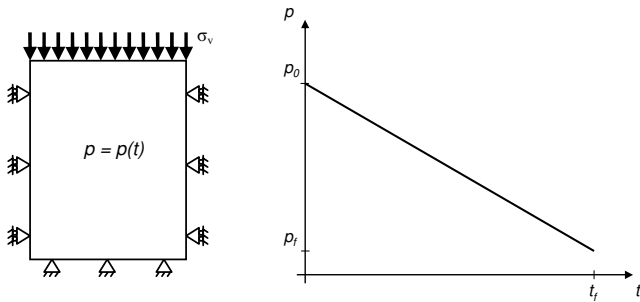
Fig. 6. Boundary conditions and pore pressure drawdown during the numerical compaction simulation.

reservoir *in situ* conditions. The specimen is constrained laterally on the vertical boundaries and fully constrained at the bottom. The pore pressure is linearly reduced (Fig. 6), which increases the effective stresses acting on the specimen and induces compaction of the reservoir rock in a similar manner to a standard compaction test, where the applied vertical load is increased under drained conditions.

The compaction simulation has two main assumptions, both of which are commonly adopted in practical reservoir engineering:

- the material deforms uniaxially (vertical compaction only),
- the total vertical stress acting on the material does not change during reservoir production (no stress arching).

Coupled and non-coupled results

The results are presented for a large reservoir where the ratio of horizontal extension to reservoir thickness is high, which is representative of most field cases. The procedure is equally valid for small and thin reservoirs, which are more prone to show stress arching for a large range of reservoir material stiffness as explained earlier, and also to deviate from uniaxial deformation.

Figure 7a shows the stress and yield surface evolution during the material compaction test, and Figure 7b plots the PVM table resulting from the experiment. Note that the material is normally consolidated and plastic compaction is occurring from the onset of the experiment. For this reason, the elastic results shown earlier (in Effect of reservoir geometry and material properties on reservoir stress path) are not directly applicable.

Figure 8a compares the coupled results with the non-coupled predictions conditioned using a constant PVM table for the reservoir. The non-coupled simulation overestimates

the pore pressure relative to the coupled prediction. The main reason for this difference is that production from a very soft reservoir (compared to the bounding material) causes stress arching, which reduces the vertical total stress acting on the reservoir and the pore pressure support provided by compaction drive. Stress arching and the associated reduction in pore pressure support are captured by the coupled model, but the non-coupled simulation overestimates the compaction driven pore pressure.

The PVM table can be adapted to account for the stress arching and the associated decrease in total vertical load acting on the reservoir. According to the coupled results, the stress arching parameter γ_v is, on average, 0.4. The numerical compaction test is repeated with an upper vertical load that reduces linearly during pore pressure drawdown according to $\gamma_v=0.4$ as shown in Figure 9. Since the vertical stress reduces during pore pressure drawdown, the rock compacts less, obtaining the new PVM table shown in Figure 10b, which incorporates the average effect of stress arching.

The new PVM table that introduces the effect of stress arching improves the non-coupled results, producing an average pore pressure drawdown much closer to the coupled pore pressure profile as shown in Figure 8b.

The stress arching effect is not homogeneous throughout the reservoir, and, for example, it can be stronger at the boundaries of the reservoir, and depend on the location of the well and the materials. A more realistic non-coupled approach would be to divide the reservoir in sectors according to the distribution of stress arching, quantified by γ_v, and use different PVM tables accordingly.

The PVM tables may also be improved by using a more general lateral boundary condition in the numerical compaction test, with a prescribed horizontal stress that linearly varies with pore pressure drawdown according to γ_h. Care should be taken, however, with the evolution of the out-of-plane horizontal stress.

The stress path parameters can be obtained based on look-up tables similar to those presented in the section on the effect of reservoir geometry and material properties on reservoir stress path, which provide the parameters suitable for a specific geometry and set of materials. If these are not available, a preliminary fluid flow-geomechanics coupled analysis may be used to locate areas that deviate from standard non-stress arching and uni-dimensional compactional behaviour, and therefore enable redefinition of the PVM tables for these regions based on the modified 1D compaction tests. This approach is suitable to improve fluid flow simulations in reservoirs with intermediate complexity. A more general approach is the use of spatially varying PVM tables for the
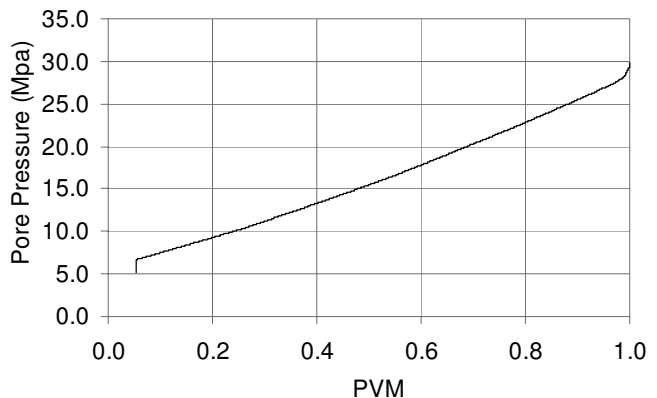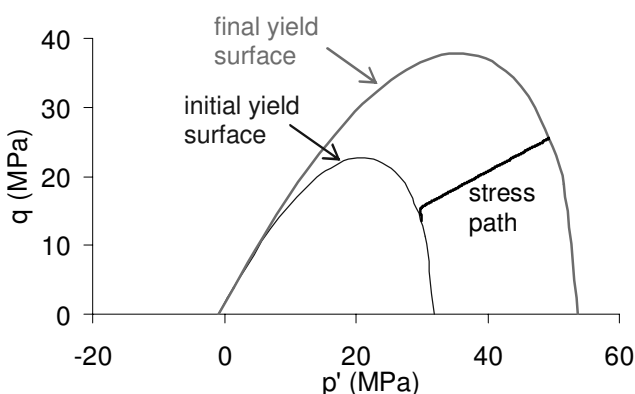

Fig. 7. Numerical compaction test results: (a) stress path in $p'-q$ plane; (b) PVM table.
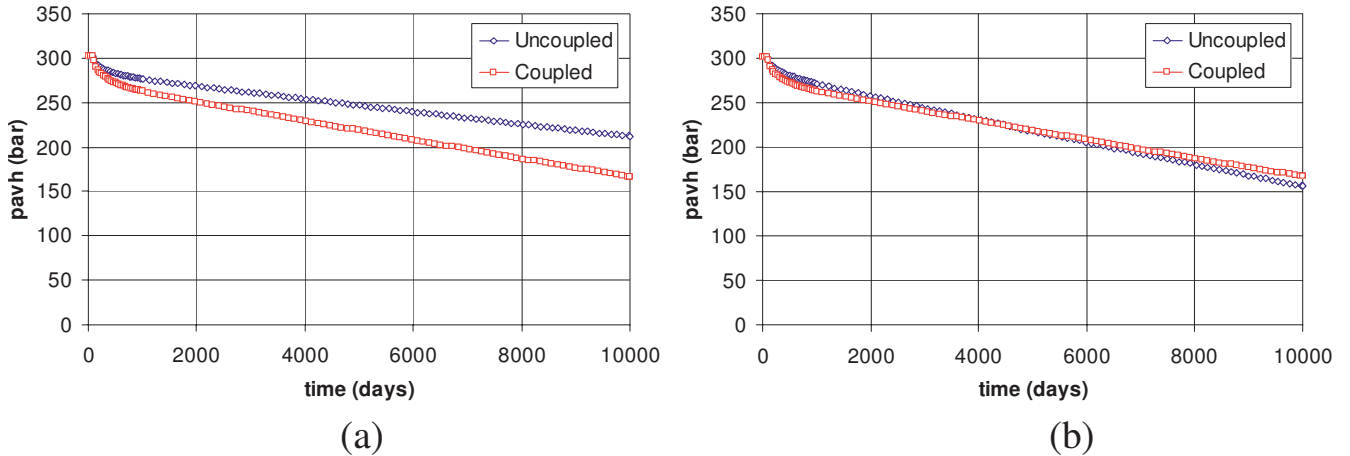
Fig. 8. Predicted average reservoir pressure using coupled v. non-coupled solutions. (**a**) PVM table without stress arching effect; (**b**) PVM table with average stress arching effect.

stand-alone reservoir simulation that are computed directly from coupled simulations (Pettersen 2008; Pettersen & Kristiansen 2009).

CONCLUDING REMARKS

This paper has extended previous work on stress path analysis to 3D reservoir geometries and has examined the key controls on reservoir stress path during production including 3D reservoir geometry and the contrast in elastic properties between the reservoir and the bounding material. The reservoir stress path is defined in terms of the stress arching parameter, γ_v, that quantifies the amount of stress arching occurring during reservoir production, and the deviatoric stress path parameter, K, which quantifies the amount of stress anisotropy developed during production. For the range of material properties analysed, the stress path parameters depend on the Young's
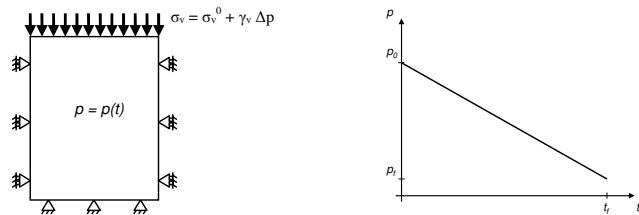

Fig. 9. Modified boundary conditions and pore pressure drawdown during the modified numerical compaction simulation.

modulus contrast between the reservoir and the bounding material independently of the Young's moduli absolute values. Stress anisotropy reduces with the bounding material Young's modulus, especially for reservoirs with low aspect ratios, but as the reservoir extends in one or the two horizontal directions, K tends to the oedometric value governed by the reservoir Poisson's ratio. Special attention is paid to the stress arching effect, which is important in low aspect ratio reservoirs that are softer than the bounding material. Stiff reservoirs compared to the bounding material show negligible stress arching independently of the geometry.

A simple methodology is also presented to increase the accuracy of non-coupled reservoir flow simulations by introducing the effect of the stress path parameters in the evaluation of look-up tables of pore volume multipliers. It is demonstrated for a rectangular reservoir that conditioning the PVM table using the stress path at the centre of the reservoir appreciably improves the accuracy of the reservoir production simulation relative to the simulation using the PVM table neglecting stress arching effects. Procedures based on this methodology have the potential to provide significant cost savings when history-matching production in complex reservoirs.
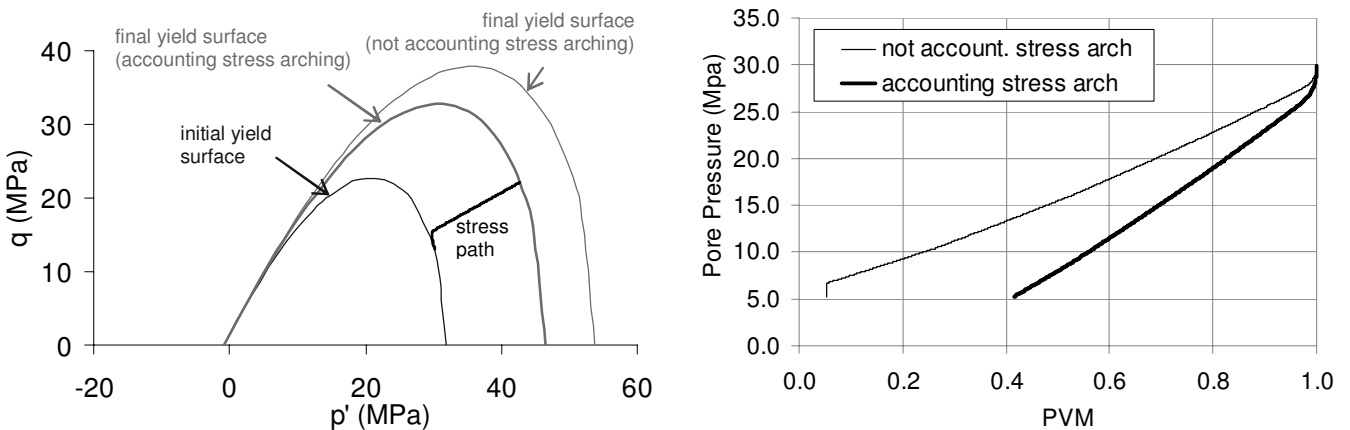
Fig. 10. Numerical compaction test results accounting including stress arching effects: (**a**) stress path in p'–q plane; (**b**) PVM table.

REFERENCES

Addis, M.A. 1997. The stress-depletion response of reservoirs, SPE 38720-MS; SPE Annual Technical Conference and Exhibition, San Antonio, Texas.

Addis, M.A., Last, N.C. & Yassir, N.A. 1996. Estimation of horizontal stresses at depth in faulted regions and their relationship to pore pressure variations. *SPE Formation Evaluation*, **11**, 11–18.

Addis, M.A., Choi, X. & Gunning, J. 1998. The influence of the reservoir stress-depletion response on the lifetime considerations of well completion design. SPE/ISRM 47289; SPE/ISRM Rock Mechanics in Petroleum Engineering, 8–10 July 1998, Trondheim, Norway.

Alassi, H.T.I., Liming, L. & Holt, R.M. 2006. Discrete element modeling of stress and strain evolution within and outside a depleting reservoir. *Pure and Applied Geophysics*, **163**, 1131–1151.

Angus, D.A., Kendall, J-M., Fisher, Q.J., Segura, J.M., Skachkov, S., Crook, A.J.L. & Dutko, M. 2010. Modelling microseismicity of a producing reservoir from coupled fluid–flow and geomechanical simulation. *Geophysical Prospecting*, **58**, 901–914.

Biot, M.A. & Willis, D.G. 1957. The elastic coefficients of the theory of consolidation. *ASME Journal of Applied Mechanics*, **24**, 594–601.

Crook, A.J.L., Yu, J.G. & Willson, S.M. 2002. Development of an orthotropic 3D elastoplastic material model for shale. *Society of Petroleum Engineers* paper 78238.

Dean, R.H., Gai, X., Stone, C.M. & Minkoff, S.E. 2003. A comparison of techniques for coupling porous flow and geomechanics. *Society of Petroleum Engineers* paper 79709; presented at the 2003 SPE Reservoir Simulation Symposium, Houston, Texas, USA.

Ervine, W.B. & Bell, J.S. 1987. Subsurface *in situ* stress magnitudes from oil well drilling records: an example from the Venture area, offshore Eastern Canada. *Canadian Journal of Earth Sciences*, **24**, 1748–1759.

Fatt, I. 1959. The Biot-Willis elastic coefficients for a sandstone. *Journal of Applied Mechanics*, **26**, 296–297.

Franquet, J.A. & Abass, H.H. 1999. Experimental evaluation of Biot's poroelastic parameter—three different methods. *In:* Amadei, B., Kranz, R.L., Scott, G.A. & Smeallie, P.H. (eds) *37th U.S. Symposium on Rock Mechanics (USRMS)*, June 7–9 Vail, CO. Balkema, Rotterdam, 349–355.

Fredrich, J.T., Arguello, J.G., Deitrick, G.L. & de Rouffignac, E.P. 2000. Geomechanical modeling of reservoir compaction, surface subsidence, and casing damage at the Belridge Diatomite Field. *SPE Reservoir Evaluation & Engineering*, **3**, 348–359.

Gai, X., Sun, S., Wheeler, M.F. & Klie, H. 2005. A timestepping scheme for coupled reservoir flow and geomechanics on non-matching grids. *Society of Petroleum Engineers* paper 97054; presented at 2005 SPE Annual Technical Conference, Dallas, Texas.

Goulty, N.R. 2003. Reservoir stress path during depletion of Norwegian chalk oilfields. *Petroleum Geoscience*, **9**, 233–241.

Gutierrez, M. & Lewis, R.W. 1998. The role of geomechanics in reservoir simulations. *Society of Petroleum Engineers/International Society of Rock Mechanics* paper 47392; presented at 1998 SPE/ISRM Eurock'98 Trondheim, Norway.

Hettema, M.H.H., Schutjens, P.M.T.M., Verboom, B.J.M. & Gussinklo, H.J. 1998. Production-induced compaction of sandstone reservoirs: the strong influence of field stress. *Society of Petroleum Engineers* paper 50630; presented at the 1998 SPE European Conference, The Hague, The Netherlands.

Hillis, R.R. 2001. Coupled changes in pore pressure and stress in oil fields and sedimentary basins. *Petroleum Geoscience*, **7**, 419–425.

Holditch, S.A., Robinson, B.M. & Whitehead, W.S. 1987. The analysis of complex Travis Peak Reservoirs in East Texas. *Society of Petroleum Engineers* paper 16427; presented at the 1987 Low Permeability Reservoir Symposium, Denver, CO.

Jones, M.E. 1994. Mechanical principles of sediment deformation. *In:* Maltman, A. (ed.) *The Geological Deformation of Sediments*. Chapman & Hall, London, 37–71.

Khan, M. & Teufel, L.W. 1996. Prediction of production-induced changes in reservoir stress state using numerical model. *Society of Petroleum Engineers* paper 36697; presented at the 1996 SPE Annual Technical Conference and Exhibition, Denver.

Khan, M., Teufel, L.W. & Zheng, Z. 2000. Determining the effect of geological and geomechanical parameters on reservoir stress path through numerical simulation. *Society of Petroleum Engineers* paper 63261; presented at the 2000 SPE Annual Technical Conference and Exhibition, Dallas, Texas, USA.

Kristiansen, T.G. 2009. Computational mechanics based workflow and toolkit to manage deformable reservoir developments, *Society of Petroleum Engineers* paper 124131; presented at SPE Offshore Europe Oil and Gas Conference, Aberdeen, UK.

Osorio, J.G., Chen, H.-Y. & Teufel, L.W. 1999. Numerical simulation of the impact of flow-induced geomechanical response on the productivity of stress-sensitive reservoirs. *Society of Petroleum Engineers* paper 51929; presented at SPE Reservoir Simulation Symposium, Houston, Texas.

Palmer, I., Ispas, I., Higgs, N., Moschovidis, Z., Patillo, P., Smith, B. & Beecroft, W. 2002. Stressman website to screen for potential geomechanical problems due to depletion. *Society of Petroleum Engineers* paper 73741; presented at SPE International Symposium and Exhibition on Formation Damage Control, Louisiana, USA.

Pettersen, Ø. 2008. Using relations between stress and fluid pressure for improved compaction modelling in flow simulation and increased efficiency in coupled rock mechanics simulation. *Petroleum Geoscience*, **14**, 399–409.

Pettersen, Ø. & Kristiansen, T.G. 2009. Improved compaction modeling in reservoir simulation and coupled rock mechanics/flow simulation, with examples from the Valhall Field. *SPE Reservoir Evaluation & Engineering*, **12**, 329–340.

Pouya, A., Djéran-Maigre, I., Lamoureux-Var, V. & Grunberger, D. 1998. Mechanical behaviour of fine grained sediments: experimental compaction and three-dimensional constitutive model. *Marine and Petroleum Geology*, **15**, 129–143.

Salz, L.B. 1977. Relationship between fracture propagation pressure and pore pressure. *Society of Petroleum Engineers* paper 6870; presented at SPE Annual Fall Technical Conference and Exhibition, Denver, Colorado.

Santarelli, F.J., Tronvoli, J.T., Svennekjaer, M., Skeie, H., Henriksen, R. & Bratli, R.K. 1998. Reservoir stress path: the depletion and the rebound. *Society of Petroleum Engineers/International Society of Rock Mechanics* paper 47350; presented at the SPRE/ISRM Eurock'98 held in Trondheim, Norway.

Sayers, C.M. 2006. Sensitivity of time-lapse seismic to reservoir stress path. *Geophysical Prospecting*, **24**, 369–380.

Sayers, C.M. & Schutjens, P.M.T.M. 2007. An introduction to reservoir geomechanics. *The Leading Edge*, May 2007, 597–601.

Segura, J.M. & Carol, I. 2008. Coupled HM analysis using zero-thickness interface elements with double nodes. Part I: Theoretical model. *International Journal for Numerical and Analytical Methods in Geomechanics*, **32**(18), 2083–2101.

Settari, A. & Walters, D.A. 1999. Advances in coupled geomechanical and reservoir modelling with applications to reservoir compaction. *Society of Petroleum Engineers* paper 51927; presented at 1999 Reservoir Simulation Symposium, Houston, Texas.

Settari, A., Sullivan, R. B., Rother, R. J. & Skinner, T. K. 2009. Comprehensive coupled modeling analysis of stimulations and post-frac productivity—case study of a tight gas field in Wyoming. *Society of Petroleum Engineers* paper 119394-MS; presented at SPE Hydraulic Fracturing Technology Conference, The Woodlands, Texas.

Shepherd, M. 1991. The Magnus Field, Blocks 211/7a, 12a, UK North Sea. *In:* Abbotts, I.L. (ed.) *United Kingdom Oil and Gas Fields. 25 Years Commemorative Volume*. Geological Society, London, Memoir **14**, 153–157.

Schutjens, P.M.T.M., Hanssen, T.H., Hettema, M.H.H., Merour, J., de Bree, P., Coremans, J.W.A. & Helliesen, G. 2004. Compaction-induced porosity/permeability reduction in sandstone reservoirs: Data and model for elasticity-dominated deformation. *Society of Petroleum Engineers* paper 88441; presented at the 2001 SPE Annual Technical Conference and Exhibition, New Orleans, USA.

Terzaghi, K. 1943. *Theoretical Soil Mechanics*. John Wiley and Sons, New York.

Teufel, L.W., Rhett, D.W. & Farrell, H.P. 1991. Effect of reservoir depletion and pore pressure drawdown on *in situ* stress and deformation in the Ekofisk field, North Sea. *In:* Roegiers, J.C. (ed.) *Rock Mechanics as a Multidisciplinary Science*. Balkema, Rotterdam, 63–72.

Tran, D., Nghiem, L. & Buchanan, L. 2005. Improved iterative coupling of geomechanics with reservoir simulation. *Society of Petroleum Engineers* paper 93244; presented at the 2005 SPE Reservoir Simulation Symposium, Houston, Texas.

Van Eijs, R.M.H.E., Mulders, F.M.M., Nepveu, M., Kenter, C.J. & Scheffers, B.C. 2006. Correlation between hydrocarbon reservoir properties and induced seismicity in the Netherlands. *Engineering Geology*, **84**, 99–111.

Verdon, J.P., Angus, D.A., Kendall, J.M. & Hall, S.A. 2008. The effect of microstructure and nonlinear stress on anisotropic seismic velocities. *Geophysics*, **73**, 206–216.

Verdon, J.P., Kendall, J.M., White, D.J., Angus, D.A., Fisher, Q.J. & Urbancic, T. 2010. Passive seismic monitoring of carbon dioxide storage at Weyburn. *The Leading Edge*, **29**, 200–206.

Winter, D.A. & King, B. 1991. The West Sole Field, Block 48/6, UK North Sea. *In:* Abbotts, I.L. (ed.) *United Kingdom Oil and Gas Fields. 25 Years*

Commemorative Volume. Geological Society, London, Memoir **14**, 517–523.

Wu, B., Addis, M.A. & Last, N.C. 1998. Stress estimation in faulted regions: the effect of residual friction. SPE-ISRM 47210; SPE/ISRM Eurock '98, Trondheim, Norway.